ACS APPLIED MATERIALS & INTERFACES

Research Article

www.acsami.org

Temperature-Stable and Optically Transparent Thin-Film Zinc Oxide Aerogel Electrodes As Model Systems for 3D Interpenetrating Organic–Inorganic Heterojunction Solar Cells

Michael Krumm, Fabian Pawlitzek, Jonas Weickert, Lukas Schmidt-Mende, and Sebastian Polarz*

University of Konstanz, 78457, Konstanz, Germany

Supporting Information

ABSTRACT: Novel, nanostructured electrode materials comprising porous ZnO films with aerogel morphology are presented. Almost any substrate including polymers, metals, or ceramics can be coated using a method that is suitable for mass production. The thin, porous films can be prepared from the wet gels via conventional drying, supercritical drying is not necessary. The filigree ZnO network is thermally very stable and exhibits sufficient electrical conductivity for advanced electronic applications. The latter was tested by realizing a highly desired architecture of organic–inorganic hybrid solar cells. After sensitizing of the ZnO with a purely organic squarine dye (SQ2), a nanostructured, interpenetrating 3D network of the inorganic semiconductor (ZnO) and organic semiconductor (P3HT) was prepared. The solar cell device was tested under illumination with AM 1.5G solar light (100 mW/cm^2) and exhibited an energy conversion efficiency (η_{eff}) of 0.69%.

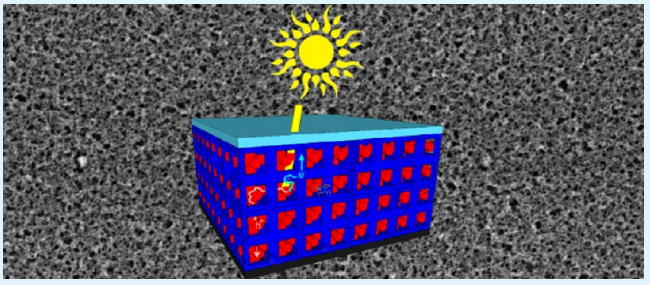

KEYWORDS: *metal oxides, nanostructured surfaces, semiconductors, hybrid materials, porous thin films, photovoltaics*

INTRODUCTION

Hybrid materials and in particular organic–inorganic hybrids represent a fascinating class of compounds.[1,2] The ongoing activity in this field is not only driven by the almost unlimited number of possible combinations of different materials but first and foremost by the hope to find new, synergistic properties.[3] This means that a hybrid material exhibits a functionality that none of its single components has on its own. A good example for the emergence of new properties for hybrids can be seen in one field of contemporary importance: Photovoltaics. The combination of a p-type and n-type semiconductor results in the formation of a charge depletion zone and an electric field across the interface which can spatially separate photoexcited bound electron–hole pairs (so-called excitons).

It is therefore a tempting idea to achieve a significant enlargement of the p/n interface. Obviously this requires a structuring of the interface preferably on the nanoscale. The preparation of nanostructured solar cells has proven to be very difficult for the classical system which is the p-/n-silicon bulk heterojunction, and also different physical principles have to be taken into consideration.[4−6] Consequently, it is worth considering alternative semiconductor systems which can be equipped very well with high-surface to volume ratio. There has been a great deal of work devoted to the synthesis of various nanoporous materials and in particular metal oxides can be prepared quite easily.[7−9] Either agglomerates of nanoparticles form a porous structure or porosity is generated via sol–gel chemistry performed in the presence of a template. A lot of attention was devoted to titanium dioxide (TiO_2). However, because TiO_2 is an indirect wide-gap semiconductor (E_{gap} = 3.2 eV for anatase) and, in addition, doping is relatively difficult to achieve, organic–inorganic hybrid heterojunctions have been applied in order to achieve both significant absorption of visible light in the organic compound and charge separation at the hybrid interface. It is worth mentioning the pioneering work of Graetzel and co-workers who have sensitized the surfaces of nanoscaled TiO_2 with organic dyes capable of absorption over a broad range of the solar spectrum.[10−12] Despite the enormous development of dye-sensitized solar cells during the past decade,[13,14] there are still two inevitable problems. The system comprises a liquid electrolyte containing a redox shuttle making the system vulnerable to leakage or evaporating, and the TiO_2 is an excellent photocatalyst which with time decomposes the surface attached dyes. Thus, there is a large interest in solvent-free hybrid solar cells using a less photoreactive combination of materials. The first condition can be fulfilled by using conducting polymers like polythiophene derivatives for light harvesting and hole conduction.[15] Because the stability of polymer-based solar cells is still a major issue,[16] at a similar band gap energy compared to TiO_2, zinc oxide (ZnO; E_{gap} = 3.3 eV) represents a promising candidate for the inorganic phase due to its significantly lower photocatalytic activity and

Received: August 4, 2012
Accepted: November 29, 2012
Published: November 29, 2012

   dx.doi.org/10.1021/am302458n | ACS Appl. Mater. Interfaces 2012, 4, 6522–6529

higher electron mobility compared to TiO_2.[17−19] In these organic−inorganic hybrid devices, the metal oxide phase becomes the electron conducting and hole blocking part, allowing the realization of the inverted bulk heterojunction (BHJ) architecture.[20,21] Because of the short lifetime of excited states in organic semiconductors and the resulting limited exciton diffusion length, which is on the order of 10 nm, nanoscale separation between donor and acceptor is necessary in order to avoid exciton recombination. Besides, once separated, free electrons and holes have to be transported through acceptor and donor matrix, respectively, demanding for high charge carrier mobility and consistent transport pathways. The latter can be difficult for isolated inorganic nanoparticles dispersed in the organic matrix, an architecture which is frequently used in hybrid inorganic−organic photovoltaic devices.[22−26] It has been realized that the allocation of an interconnected pathway is beneficial for an effective transport the photogenerated charge carriers. Therefore, there was significant interest in the use of more refined ZnO nanostructures in photovoltaic devices.[27−30] Major attention was devoted to ZnO nanorods because there is a large chance for percolation and, thus, for the formation of a suitable electronic path.[31−33] Furthermore, it has been reported that branched structures like tetrapods present improved pathways for electron transport through their intertwining character.[25,34−37] However, for the successful dispersion of the inorganic particles in the continuous (organic) phase, surface modification with organic groups like alkyl chain surfactants is typically required. The resulting, electrically insulating layer could hamper the electron transfer to the inorganic phase and between the particles. Considering the latter arguments, the materials architecture shown in Scheme 1 is generally proposed as the ideal one.[38]

The key element is a porous and transparent metal oxide film consisting of a continuous phase of highly crystalline hyperbranched and electrically interconnected nanoparticles. Exactly this refined architecture is realized in the current paper, and it is studied if positive effects concerning the photovoltaic performance can be observed.

RESULTS AND DISCUSSION

Preparation of Crystalline ZnO Aerogel Electrodes. Recently we were able to establish a reliable sol−gel process for ZnO using organometallic precursors leading to nanocrystalline aerogels with monolithic shape.[39] These precursors have already proven their versatility regarding the preparation of different ZnO materials in the past.[40−48] The preparation of thin aerogel films represents a valuable goal since others have argued for porous materials in general that additional functionality can be gained from of a thin-film architecture.[49] Since the formation of the ZnO aerogel in liquid dispersion involves a mechanism with temporally distinctive sol and gelation steps,[39] there is a narrow time window to yield homogeneous coating of the substrate with a thin aerogel film via dip-coating. The as prepared, wet films were dried conventionally via solvent evaporation at room temperature followed by a treatment at 100 °C. While it is known that bulk aerogel materials tend to collapse under conventional drying conditions,[50] the examination of the resulting materials via scanning electron microscopy (SEM) showed that the desired filigree and porous structure was present (Figure 1).

Thus, a step comprising an elaborate supercritical solvent exchange is not necessary for retaining the aerogel structure

Scheme 1. Illustration of the Advanced Architecture for Organic−Inorganic Hybrid, Inverted Bulk-Heterojunction Solar Cells As Realized in the Current Paper[a]

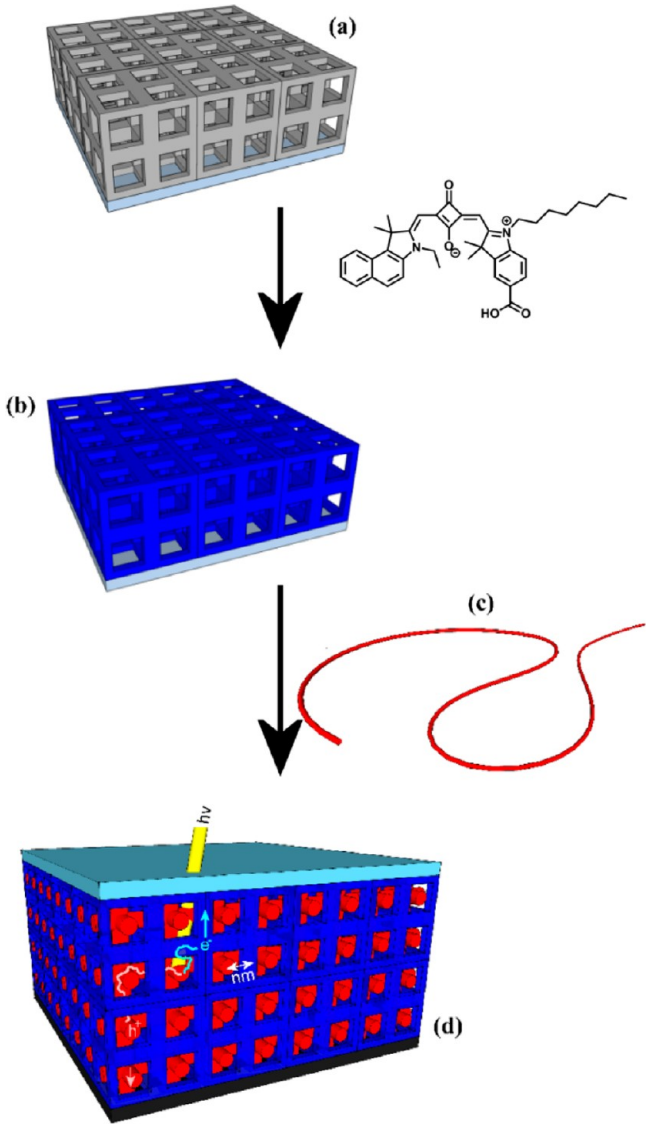

[a](a) A novel nanostructured electrode comprising a thin film of a highly porous zinc oxide network (grey) on ITO (light blue) is sensitized with an organic dye (SQ2), resulting in (b) the surface-modified material (illustrated with the blue color) and (c) combined with conducting, organic polymers like poly-3-hexylthiophene (red). (d) Charge carriers created because of the absorption of light are separated more effectively due to enforced, spatial proximity of the hole-conducting, organic phase, and the electron-conducting ZnO phase.

which is a major advantage. Large areas of a homogeneous and highly porous thin aerogel film can be prepared (see also the Supporting Information SI-1). The described method is applicable to a broad range of different inorganic materials such as metal foils, glass substrates, metal oxides, and for organic and flexible substrates such as polyvinylchloride foils (see Figure 2).

Because of the nature of the aerogel structure the pore-size distribution is very broad, beginning with accessible macropores. The majority of pores have diameters well below 100 nm. As previously reported, the surface area of the bulk-

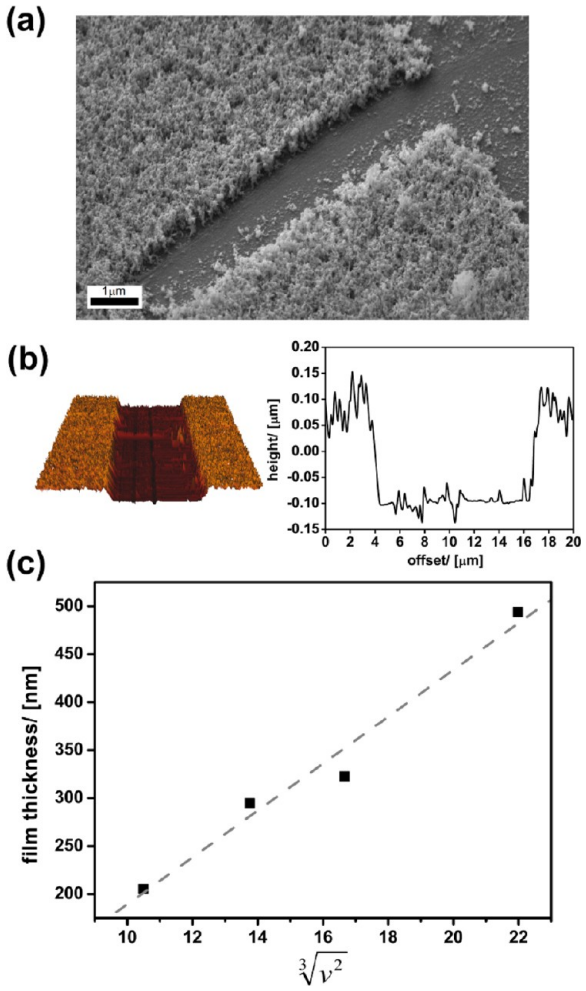

Figure 1. (a) SEM and (b) AFM height-profile evaluation of a 200 nm thin ZnO aerogel film. The film was carved to determine the film thickness. (c) Experimental data for film thickness (black data points) in comparison to the Landau−Levich equation (gray line).

materials is in the range 130−150 m^2/g.[39] For thin aerogel films scratched from a glass substrate a surface area of over 80 m^2/g could be determined via N_2 physisorption measurements (see SI-2 in the Supporting Information). Besides porosity, other parameters are expected to influence the performance of the porous thin film electrodes, namely film thickness, crystallinity and electrical conductivity. The transport efficiency of free charge carriers within the semiconductor is an important factor regarding electronic applications and is enhanced by increasing the crystallinity of the material.

The as prepared films were investigated using grazing-incidence powder X-ray diffraction (PXRD) (see Figure 3; for scattering range below 25° 2θ, see SI-3 in the Supporting Information). Weak signal intensities are found, which are attributed to the low crystallinity of the as-prepared material. The crystallinity could be enhanced significantly by treating the films at elevated temperatures for several hours. The crystallization process is documented by the emergence of the characteristic ZnO pattern in the PXRD diffraction patterns shown in Figure 3. However, it is of elemental importance to prove that the aerogel morphology remains unaffected by the sintering procedure. The N_2 physisorption isotherm of ZnO aerogel films before and after sintering at 400 °C for several hours are revealing a loss of BET surface area from 82.7 to 46.6 m^2/g (see SI-2 in the Supporting Information). This is due to the conversion of amorphous domains to crystalline domains and the growth of the crystallites (4.7 nm → 7.4 nm) as proven by PXRD. It is remarkable that the aerogel morphology is still existent and no visible shrinkage or crumbling of the filigree structure could be observed by comparing the SEM images before and after sintering of a 200 nm thick aerogel film. (Figure 3). A high-resolution transmission electron microscopy (HRTEM) image of the aerogel film after the temperature treatment shown in Figure 4 reveals that the nanocrystals are highly crystalline and in good contact to each other.

Besides the crystallinity another important material characteristic is the film thickness influencing the optical as well as some important electronic characteristics. For example, in hybrid solar cells, the film thickness of the electron transporting layer directly affects the travel length of the free charges to the electrode and the photon absorption efficiency because of polymer loading. Finding an effective way to adjust the film thickness is fundamental to guarantee an efficient fabrication of such devices. The film thickness h was measured using a combination of SEM and atomic force microscopy (AFM) height profile analysis (see Figure 1b) upon which the effect of the withdrawal rate v during the dip-coating process was investigated. The data were evaluated using the so-called Lindau−Levich equation[51,52]

$$h = 0.94\frac{(\eta v)^{2/3}}{\gamma_{LV}^{1/6}(\rho g)^{1/2}} \quad (1)$$

with $\eta \cong$ viscosity of the solution, $\gamma_{LV} \cong$ liquid−vapor surface tension, $\rho \cong$ density, g ≅ gravity. Thus, a plot h versus the cubic root of v^2 should result in a linear graph. The excellent agreement to the Landau-Levich behavior proves that the thickness of the aerogel-films can be adjusted very precisely starting from 200 nm up to several micrometers (see SI-4 in the Supporting Information). The films are transparent in the entire VIS-region which can be seen from UV/vis spectroscopy (data given in SI-5 in the Supporting Information). Only in the UV (λ = 360 nm) is the absorption edge due to the band gap of ZnO. The good homogeneity, chemical purity, and outstanding quality of the films are also apparent from their visual transparency. Photographic images of a glass-cover slide coated with a 200 nm aerogel film are shown in SI-5 in the Supporting Information and Figure 2. No organic or carbonaceous impurities were present which could be seen from energy dispersive X-ray spectroscopy (EDX) (see SI-6 in the Supporting Information). The material presented here is thus unique and superior to other reported ZnO electrode coatings.[53−55]

Hybrid BHJ Solar Cells. The prepared aerogel ZnO films were applied as porous electrodes in solar cells. First, a compact, 100 nm thick ZnO film was deposited on conducting ITO glass by RF magnetron sputtering as a hole blocking and shortcut preventing protection layer. Different film thicknesses were made possible by prolonging the deposition time. The resulting ZnO films thicknesses were measured by (AFM) height profile analysis and plotted versus the deposition time, resulting in a linear graph (shown in SI-7 in the Supporting Information). In the next step, ZnO aerogel films with the desired film thickness were prepared on top followed by annealing of the films to increase the crystallinity.

The ZnO materials can either be used as prepared, or one can modify the surfaces with an additional, light-absorbing

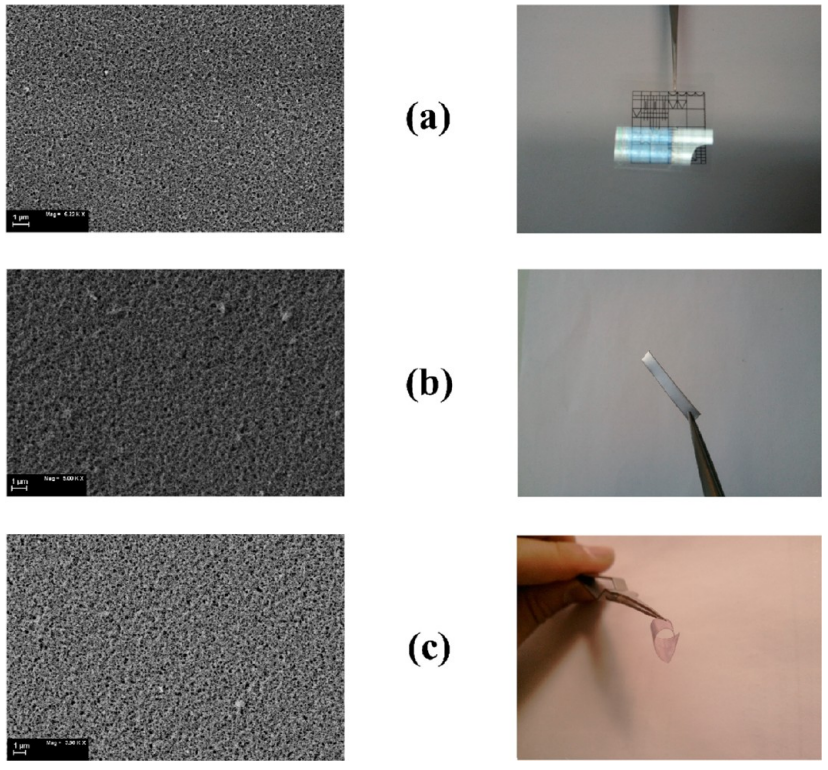

Figure 2. Different materials coated with 200 nm thin ZnO aerogel-film. (a) Glass slide, (b) titanium foil, (c) on flexible PVC-foil (the SEM image shows the thin film prior to polymer infiltration and the photograph shows the film after infiltration, which was chosen for better visibility because of the coloration caused by the presence of P3HT).

entity. Others have reported recently, that enhanced light absorption and better efficiencies of BHJ solar cells can be realized for sensitizing the surfaces of the metal oxide with dye molecules.[56−59] Therefore, we have also used the organic squarylium cyanine dye SQ2 (see SI-8 in the Supporting Information) for immobilization on the ZnO aerogel films. A solution of the conducting polymer poly(3-hexylthiophene) (P3HT) has been spin-cast onto the aerogel film. A layer of poly(3,4-ethylenedioxythiophene)-poly(styrenesulfonate) (PEDOT:PSS) was deposited via combination of spray and spin-casting to yield a homogeneous film. The cell was finalized by the air stable silver (Ag) counter-electrode. The successful infiltration of the polymer was shown as follows. A cross-section of an edge created by cutting was investigated with SEM (Figure 5). The filigree nature of the aerogel cannot be seen anymore as if the polymer has filled all voids of the porous ZnO network. That the network is still present can be demonstrated by removal of the polymer via ozone treatment at elevated temperatures. The SEM images of the resulting material shows the same aerogel morphology as prior to polymer infiltration (see SI-9 in the Supporting Information). The realized high degree of intermixing between the polymer and the metal oxide promotes short travel lengths from the site of charge generation trough the organic phase, thus avoiding recombination processes and therefore leading to more efficient charge separation.

BHJ solar cells fabricated with 300 nm thick, sintered ZnO aerogel films were compared to devices with nonsintered aerogel films of the same film thickness regarding their performance under illumination with simulated AM 1.5G solar light (100 mW/cm^2). In agreement to the literature,[56−59] we could also see that the SQ-2 sensitized materials exhibit better performance compared to the pure ZnO materials. Therefore, we have concentrated on the SQ-2 containing materials. The current−voltage characteristics of both devices are shown in Figure 6. It can be shown that electrons can also be transported efficiently enough through nonsintered ZnO. The latter finding is important for the preparation of aerogel-like ZnO films on substrates which do not withstand high temperatures like polymer foils. However, the energy conversion efficiency η_{eff} = 0.33% is relatively low. Charge mobility is higher in the temperature-treated films due to the enhanced crystallinity, larger domain size and better contact between the ZnO grains (Figure 4). This directly leads to a much better value for η_{eff} = 0.54%.

Besides crystallinity, the film thickness of the ZnO aerogel layer could also have an impact on the performance of the solar cells. To investigate the effect of varying film thickness, we tested the optical as well as the solar cell performance characteristics. In SI-10 in the Supporting Information, the UV−vis spectra of the prepared solar cells with varying thickness from 200 to 500 nm are pictured. As expected, the absorption in the UV region increases with increasing ZnO aerogel layer thickness. The increasing absorption of P3HT in the region from 580 to 400 nm is slightly enhanced with increasing aerogel film thickness because of the higher amount of polymer. This effect is more pronounced regarding the absorption of the SQ2 dye at 675 nm, where a big difference between the 500 nm and the 200 nm, respectively, 300 nm, can be observed. When the solar cells are built and their performance is tested, there is a linear increase in the solar cell energy conversion efficiency with declining film thickness from 500 to 200 nm (Figure 7a; see SI-11 in the Supporting Information). This trend is easily explained considering the

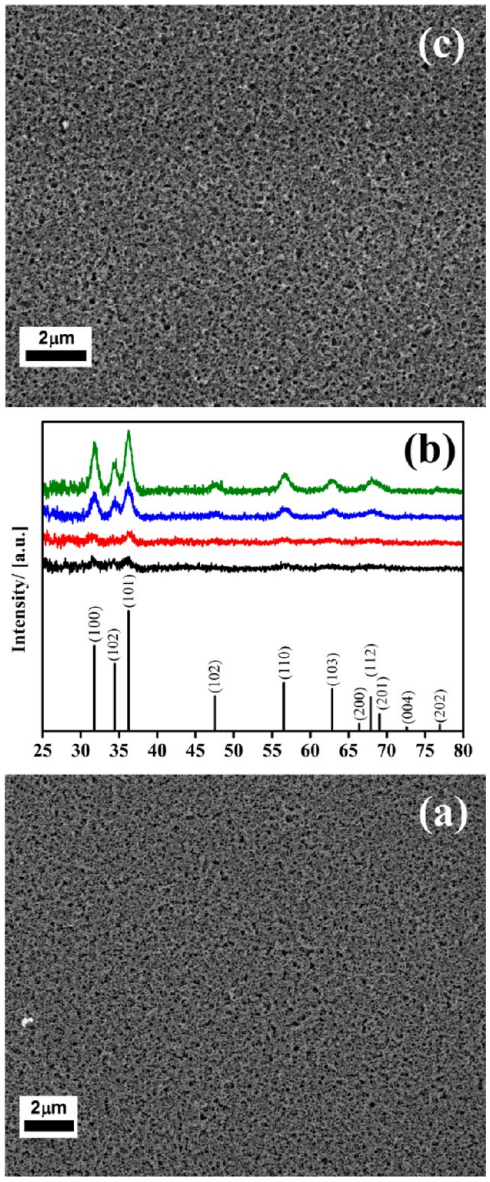

Figure 3. SEM images of thin aerogel films (a) before and (c) after sintering (T = 400 °C). (b) GI-PXRD data for different sintering temperatures; 100 °C (as-prepared material; black graph), 200 °C (red graph), 300 °C (blue graph), 400 °C (green graph). The reference pattern of bulk ZnO is shown as black bars.

EQE spectra shown in Figure 7b. Although in the case of the thicker films there is more of the active layer present to absorb the incoming photons, less of the separated charges are collected at the electrodes, because of the limited penetration depth of the light into the material combined with the longer travel length of the charges and therefore higher chance for recombination. This results in overall lower EQE values and lower energy conversion efficiencies with increasing film thickness.

The current−voltage characteristic and the EQE spectra of the solar cell with a sintered 200 nm thick aerogel layer are shown in Figure 8. The cells reach rather high values for the short circuit current I_{sc} = 3.78 mA/cm^2 because of the high absorption yield of the incident photons over the whole spectral range from 350 nm to 750 nm shown in the EQE spectrum leading to generation of separated charges with a

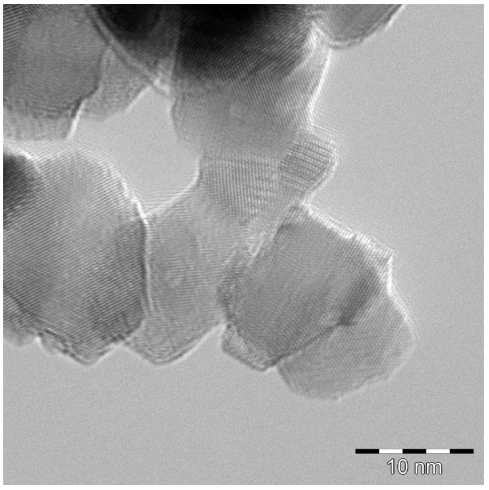

Figure 4. HRTEM image of a highly crystalline thin aerogel film obtained after heating to 400 °C for 4 h. The visible index planes correspon to the (100) of ZnO (d = 0.28 nm).

maximum of 21.6% at a wavelength of 517 nm. The value for the open circuit voltage (V_{oc} = 0.37 V) shows, that the generated charges are successfully separated and are able to travel through the interconnected structure of the ZnO aerogel to the electrodes. This results in a fill factor of 50.2% with an efficiency of η_{eff} = 0.69%.

Because of the novelty of the concept using highly porous and interconnected aerogel electrodes sensitized with organic dye it is difficult to compare these values to the ones existing in the literature. Best comparable to our system are BHJ geometries with different ZnO nanomaterial/P3HT blends. The reported efficiencies are ranging from 0.2% for dye-sensitized nanorod arrays,[31] to 0.35% for nanostructured ZnO[60] and 0.53%[61] for ZnO fibers. The highest reported efficiency using a different approach with a novel precursor method was reported by Janssen et al. reaching η = 2%.[62]

CONCLUSION

The main part of the paper was concerned with the preparation of novel nanostructured electrode materials consisting of the semiconducting metal oxide ZnO. Different substrates including ceramics, metals, and even polymer foils could be coated with a homogeneous, highly porous film of a nanocrystalline ZnO aerogel. The films are very homogeneous and their thickness could be adjusted from 200 nm to several micrometers.

Next, their use in inverted BHJ solar cells was tested. The successful interpenetration of the aerogel voids with conducting polymer after sensitizing with organic dye enabled the preparation of advanced hybrid solar cells. Especially in hybrid solar cells, where an absorbing hole transporter is used, aerogel films are potentially more attractive than nanoparticle films because of their higher porosity. The pore-size of aerogel-like materials is in an ideal size range because the pores are large enough to enable easy and effective infiltration of the polymer into the pores. At the same time the pores are small enough for granting an intimate contact between the oxide matrix and the conduction polymer. Unlike in nanoparticle systems, there is no insulating layer due to the stabilization agents needed for the nanoparticles, and phase-separation processes can be avoided. Higher porosity allows infiltration of more polymer per volume

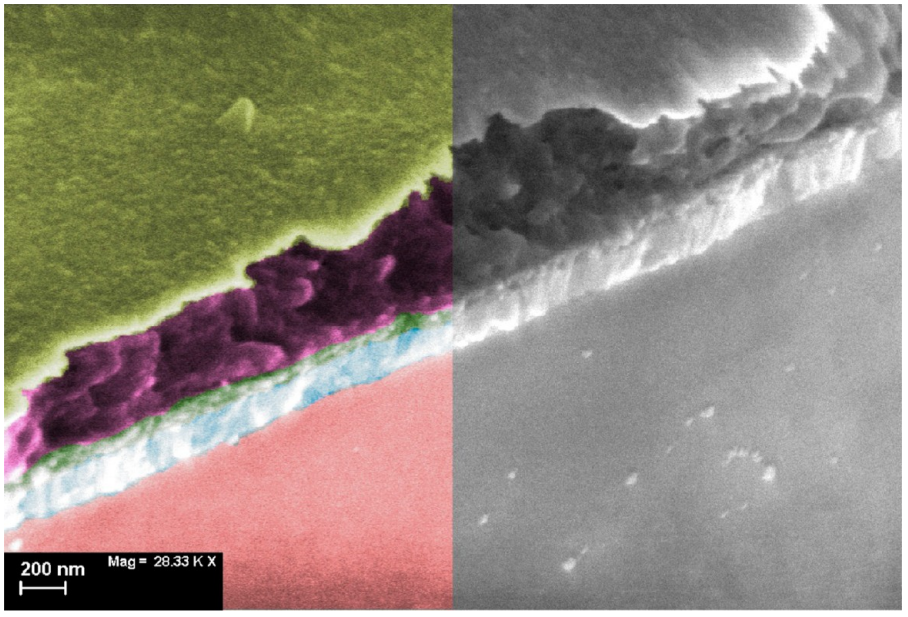

Figure 5. Color-coded SEM image of the prepared photovoltaic cell for better differentiation between the layers. Glass substrate (red), conducting ITO layer (blue), dense ZnO film (green), P3HT infiltrated into porous ZnO aerogel matrix (purple), PEDOT:PSS layer topped with thin Ag electrode (green).

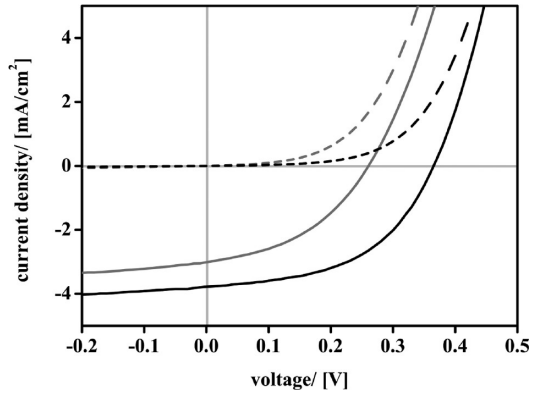

Figure 6. Current−voltage characteristic for BHJ solar cell with 300 nm ZnO aerogel layer, unsintered (gray line) and temperature-treated at 400 °C (black line) measured in the dark (dashed line) and with AM 1.5G solar light (100 mW/cm^2) (solid line).

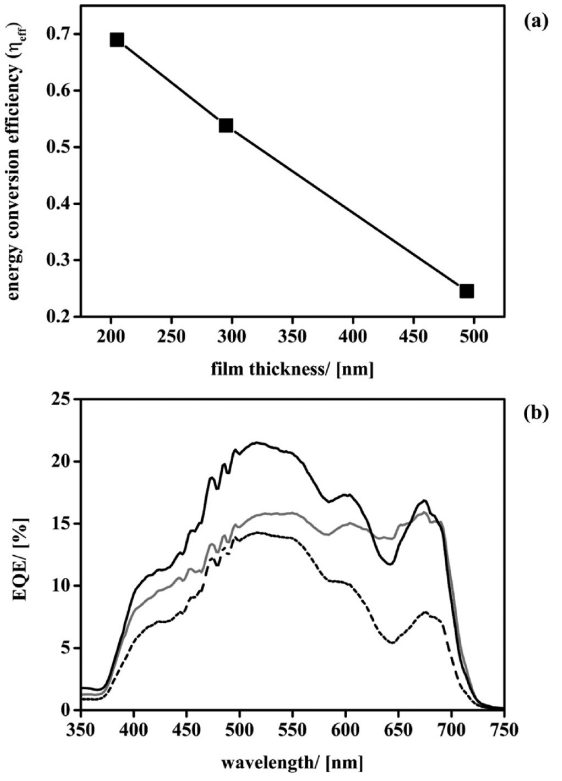

Figure 7. (a) ZnO aerogel film layer thickness plotted against energy conversion efficiency. (b) EQE spectra of BHJ solar cells with different layer thickness of aerogel film. (black line = 200 nm, gray line = 300 nm, dashed black line = 500 nm).

and thus higher extinction coefficients and more efficient light harvesting.

It was seen that aerogel films prepared at low temperature and with low crystallinity exhibit reasonable performances. Sintering of the films lead to an increase in crystallinity and better charge carrier mobility, whereas the filigree nature of the aerogel was not altered. Finally, it was shown that the film thickness is an important parameter for further optimization. Up to know the device prepared using a 200 nm thick film has the best efficiency values of η_{eff} = 0.69%. It can be expected that there will be a maximum in η_{eff} for even thinner films (see Figure 7). This and other optimizations will be done in the near future.

EXPERIMENTAL SECTION

All starting compounds were until noted otherwise received from Aldrich, purified, and carefully dried prior to use.

Preparation of ZnO Aerogel Film. In a typical synthesis, the $[MeZnO^iPr]_4$ heterocubane was dissolved under moderate heating under argon atmosphere in bis(2-methoxyethyl)ether ($c_{precursor}$ = 0.09 M). The solution was cooled to 0 °C and 4 equiv. of water were added. The solution was kept at 0 °C for 80 min to form a stable dispersion just before the gel point. The substrate are now dipped into the dispersion at 0 °C with a rate of 34 mm/min and after 60 s withdrawn at a rate corresponding to the desired film thickness of 200 nm. After

dx.doi.org/10.1021/am302458n | ACS Appl. Mater. Interfaces 2012, 4, 6522−6529

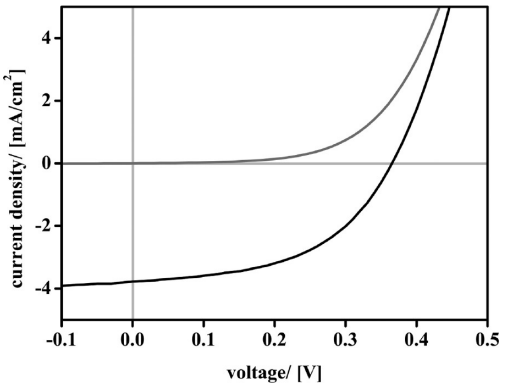

Figure 8. Current voltage characteristic and for P3HT/ZnO BHJ solar cell with 200 nm aerogel layer, temperature-treated, and sensitized with SQ2 dye.

10 min of drying at room temperature, the films were annealed by heating at 100 °C for 1 h followed by heating to 400 °C with a heating rate of 1 °C per min and afterward keeping that temperature for 4 h.

Preparation of ZnO Protection Layer. The ZnO films were deposited via RF magnetron sputtering (AJA Orion UHV-Sputter system) using a zinc target at a basic pressure of 1×10^{-7} Torr. Argon stream was adjusted to 80 sccm Argon, Oxygen stream was 10 sccm at a pressure of 2.5 mTorr. The power was set to 300 W and for the approximately 100 nm protection layer, the deposition time was adjusted to 300 s.

Characterization. X-ray diffraction was performed on a Bruker AXS D8 Advance diffractometer using Cu K_α radiation. A special measurement geometry called "grazing incidence" has been applied, where the incident radiation is fixed at small angles and only the detector is moved over the angle area, leading to an enhanced absorption of the thin film and therefore to an increase of the reflex intensities. SEM images were recorded on a Zeiss CrossBeam 1540XB scanning electron microscope. High resolution transmission electron microscopy (HRTEM) images were recorded with a JEOL, JEM 2200FS HRTEM operating with an acceleration voltage of 200 kV. AFM measurements were performed with JPK NanoWizard atomic force microscope in the intermittent contact mode using a Silicon tip with a force constant of 40 N m^{-1} and resonant frequency of about 300 kHz. Further surface analysis was performed with an Ambios XP2 Profilometer.

Solar Cell Fabrication. Solar cells were fabricated on indium–tin oxide (ITO) coated glass substrates (Kintech, 10 Ω/sq.). ITO glasses were subsequently cleaned in an ultrasonic bath with acetone, isopropanol and deionized water for 15 min each and dried in air at 60 °C. ZnO flat films of approximately 100 nm thickness, serving as protection layer, were deposited on ITO glasses as described above. On top, ZnO aerogel films with varying film thickness were prepared as described above. The films were immersed in a 2 mM solution of the squarine dye SQ2 (Solarnix) in ethanol for 60 min, excessively rinsed with ethanol and dried in a nitrogen stream. P3HT (P2000; Rieke Metals) was spin coated from a 20 mg/mL solution in chlorobenzene. Substrates were wetted with P3HT solution allowing the polymer to diffuse into the nanostructure, after 30 s the spin coating started at 1500 rpm. After spin coating, samples were annealed at 140 °C for 2 min in ambient air. Approximately 40 nm poly(3,4-ethylenedioxythiophene) poly(styrenesulfonate) (PEDOT:PSS) were spray-deposited on the P3HT films from a 1:10 diluted solution in 2-propanol as described elsewhere in detail.[63] In brief, an aqueous solution of PEDOT:PSS was used as received from HC Starck and diluted at 1:10 volume ratio in isopropanol. The solution was then sprayed onto the active layer and the sample was spincoated at 1000 rpm for 1 min. To finalize the solar cells, Ag top contacts where thermally evaporated at a pressure $<3 \times 10^{-6}$ mbar at deposition rates of 0.1–2 Å/s. Subsequently, solar cells were annealed at 140 °C for 5 min in ambient air.

Solar Cell Characterization. Current–voltage characteristics were recorded using a Keithley 2401 Sourcemeter controlled by a self-written LabView program. Solar cells were illuminated through a shadow mask and the active area was 0.125 cm^2. For characterization under simulated sunlight a LOT-Oriel LS0106 solar simulator with a Xe lamp and an AM 1.5G filter was focused onto the solar cells and adjusted to a light power of 100 mW/cm^2. For EQE measurements a Xe lamp was focused onto a monochromator resulting in light intensities of approximately 2 mW/cm^2 at 450 nm . For calibration, a Fraunhofer Institute certified Si reference solar cells with a KG5 filter was used.

■ ASSOCIATED CONTENT

Supporting Information

SI-1: Additional electron microscopy data for aerogel films, data of optical properties. SI-2: N_2 physisorption data. SI-3: GI-PXRD data of a thin aerogel film. SI-4: SEM of a thicker aerogel film. SI-5: Optical properties of a thin aerogel film. SI-6: EDX spectrum. SI-7: Height profile analysis and AFM images. SI-8: Full name and structure of SQ2. SI-9: SEM of the film after oxidative polymer removal. SI-10: UV–vis spectra of prepared solar cells. SI-11: *I*/*V* curves for solar cells comprising ZnO films with different thickness. Dye, physisorption measurements, EQE spectra, and current voltage characteristics. This material is available free of charge via the Internet at http://pubs.acs.org.

■ AUTHOR INFORMATION

Corresponding Author

*E-mail: Sebastian.polarz@uni-konstanz.

Author Contributions

M.K. has prepared and characterized the materials. F.B. has contributed during the P3HT infiltration experiments and has prepared the first solar cells. J.W. and L.S.M. have performed the photovoltaic measurements and interpreted the data. S.P. has written the paper and designed the research.

Funding

The current work was financed within the REFINE research consortium funded by the Carl-Zeiss foundation.

Notes

The authors declare no competing financial interest.

■ ACKNOWLEDGMENTS

We thank Daniel Skorka for help with the magnetron sputtering of ZnO. We thank Matthias Hagner for the introduction to SEM and Profilometer. We thank Melanie Gerigk for help with the HRTEM pictures.

■ REFERENCES

(1) Judeinstein, P.; Sanchez, C. *J. Mater. Chem.* **1996**, *6*, 511–525.
(2) Wen, J. Y.; Wilkes, G. L. *Chem. Mater.* **1996**, *8*, 1667–1681.
(3) Gomez-Romero, P. *Adv. Mater.* **2001**, *13*, 163–174.
(4) De la Torre, J.; Bremond, G.; Lemiti, M.; Guillot, G.; Mur, P.; Buffet, N. *Mater. Sci. Eng., C* **2006**, *26*, 427–430.
(5) Kayes, B. M.; Atwater, H. A.; Lewis, N. S. *J. Appl. Phys.* **2005**, *97*, 114302.
(6) Konstantatos, G.; Sargent, E. H. *Nat. Nano.* **2010**, *5*, 391–400.
(7) Polarz, S.; Smarsly, B. *J. Nanosci. Nanotechnol.* **2002**, *2*, 581–612.
(8) Schueth, F. *Chem. Mater.* **2001**, *13*, 3184–3195.
(9) Taguchi, A.; Schueth, F. *Microporous Mesoporous Mater.* **2005**, *77*, 1–45.
(10) Graetzel, M. *Nature* **2001**, *414*, 338–344.
(11) Kavan, L.; Rathousky, J.; Graetzel, M.; Shklover, V.; Zukal, A. *Microporous Mesoporous Mater.* **2001**, *44*, 653–659.

(12) Oregan, B.; Graetzel, M. *Nature* **1991**, *353*, 737−740.
(13) Graetzel, M. *J. Photochem. Photobiol. C* **2003**, *4*, 145−153.
(14) Graetzel, M. *Acc. Chem. Res.* **2009**, *42*, 1788−1798.
(15) Dimitrakopoulos, C. D.; Malenfant, P. R. L. *Adv. Mater.* **2002**, *14*, 99−117.
(16) Jorgensen, M.; Norrman, K.; Gevorgyan, S. A.; Tromholt, T.; Andreasen, B.; Krebs, F. C. *Adv. Mater.* **2012**, *24*, 580−612.
(17) Oh, H.; Krantz, J.; Litzov, I.; Stubhan, T.; Pinna, L.; Brabec, C. J. *Sol. Energ. Mat. Sol. C.* **2011**, *95*, 2194−2199.
(18) Studenikin, S. A.; Golego, N.; Cocivera, M. *J. Appl. Phys.* **2000**, *87*, 2413−2421.
(19) Boucle, J.; Ackermann, J. *Polym. Int.* **2012**, *61*, 355−373.
(20) Hau, S. K.; Yip, H. L.; Baek, N. S.; Zou, J. Y.; O'Malley, K.; Jen, A. K. Y. *Appl. Phys. Lett.* **2008**, *92*, 253301.
(21) White, M. S.; Olson, D. C.; Shaheen, S. E.; Kopidakis, N.; Ginley, D. S. *Appl. Phys. Lett.* **2006**, *89*, 143517.
(22) Beek, W. J. E.; Slooff, L. H.; Wienk, M. M.; Kroon, J. M.; Janssen, R. A. J. *Adv. Funct. Mater.* **2005**, *15*, 1703−1707.
(23) Beek, W. J. E.; Wienk, M. M.; Janssen, R. A. J. *Adv. Mater.* **2004**, *16*, 1009−1012.
(24) Beek, W. J. E.; Wienk, M. M.; Janssen, R. A. J. *Adv. Funct. Mater.* **2006**, *16*, 1112−1116.
(25) Huynh, W. U.; Dittmer, J. J.; Alivisatos, A. P. *Science* **2002**, *295*, 2425−2427.
(26) Huang, J.; Yin, Z. G.; Zheng, Q. D. *Energy Environ. Sci.* **2011**, *4*, 3861−3877.
(27) Rani, S.; Suri, P.; Shishodia, P. K.; Mehra, R. M. *Sol. Energy Mater. Sol. Cells* **2008**, *92*, 1639−1645.
(28) Djurisic, A. B.; Ng, A. M. C.; Chen, X. Y. *Prog. Quant. Electron.* **2010**, *34*, 191−259.
(29) Reeja-Jayan, B.; De la Rosa, E.; Sepulveda-Guzman, S.; Rodriguez, R. A.; Yacaman, M. J. *J. Phys. Chem. C* **2008**, *112*, 240−246.
(30) Suresh, P.; Balaraju, P.; Sharma, S. K.; Roy, M. S.; Sharma, G. D. *Sol. Energ. Mat. Sol. C.* **2008**, *92*, 900−908.
(31) Peiro, A. M.; Ravirajan, P.; Govender, K.; Boyle, D. S.; O'Brien, P.; Bradley, D. D. C.; Nelson, J.; Durrant, J. R. *J. Mater. Chem.* **2006**, *16*, 2088−2096.
(32) Ravirajan, P.; Peiro, A. M.; Nazeeruddin, M. K.; Graetzel, M.; Bradley, D. D. C.; Durrant, J. R.; Nelson, J. *J. Phys. Chem. B* **2006**, *110*, 7635−7639.
(33) Gonzalez-Valls, I.; Lira-Cantu, M. *Energy Environ. Sci.* **2009**, *2*, 19−34.
(34) Dayal, S.; Reese, M. O.; Ferguson, A. J.; Ginley, D. S.; Rumbles, G.; Kopidakis, N. *Adv. Funct. Mater.* **2010**, *20*, 2629−2635.
(35) Sun, B. Q.; Marx, E.; Greenham, N. C. *Nano Lett.* **2003**, *3*, 961−963.
(36) Thompson, B. C.; Frechet, J. M. J. *Angew. Chem., Int. Ed.* **2008**, *47*, 58−77.
(37) Yang, X. N.; Loos, J.; Veenstra, S. C.; Verhees, W. J. H.; Wienk, M. M.; Kroon, J. M.; Michels, M. A. J.; Janssen, R. A. J. *Nano Lett.* **2005**, *5*, 579−583.
(38) Moule, A. J.; Chang, L. L.; Thambidurai, C.; Vidu, R.; Stroeve, P. *J. Mater. Chem.* **2012**, *22*, 2351−2368.
(39) Krumm, M.; Pueyo, C. L.; Polarz, S. *Chem. Mater.* **2010**, *22*, 5129−5136.
(40) Polarz, S.; Pueyo, C. L.; Krumm, M. *Inorg. Chim. Act.* **2010**, *363*, 4148−4157.
(41) Lizandara-Pueyo, C.; Siroky, S.; Wagner, M. R.; Hoffmann, A.; Reparaz, J. S.; Lehmann, M.; Polarz, S. *Adv. Funct. Mater.* **2011**, *21*, 295−304.
(42) Pueyo, C. L.; Siroky, S.; Landsmann, S.; van den Berg, M. W. E.; Wagner, M. R.; Reparaz, J. S.; Hoffmann, A.; Polarz, S. *Chem. Mater.* **2010**, *22*, 4263−4270.
(43) Lizandara-Pueyo, C.; van den Berg, M. W. E.; De Toni, A.; Goes, T.; Polarz, S. *J. Am. Chem. Soc.* **2008**, *130*, 16601−16610.
(44) Polarz, S.; Roy, A.; Lehmann, M.; Driess, M.; Kruis, F. E.; Hoffmann, A.; Zimmer, P. *Adv. Funct. Mater.* **2007**, *17*, 1385−1391.
(45) Polarz, S.; Strunk, J.; Ischenko, V.; van den Berg, M. W. E.; Hinrichsen, O.; Muhler, M.; Driess, M. *Angew. Chem., Int. Ed.* **2006**, *45*, 2965−2969.
(46) Polarz, S.; Roy, A.; Merz, M.; Halm, S.; Schroeder, D.; Schneider, L.; Bacher, G.; Kruis, F. E.; Driess, M. *Small* **2005**, *1*, 540−552.
(47) Polarz, S.; Neues, F.; van den Berg, M. W. E.; Gruenert, W.; Khodeir, L. *J. Am. Chem. Soc.* **2005**, *127*, 12028−12034.
(48) Ischenko, V.; Polarz, S.; Grote, D.; Stavarache, V.; Fink, K.; Driess, M. *Adv. Funct. Mater.* **2005**, *15*, 1945−1954.
(49) Sanchez, C.; Boissiere, C.; Grosso, D.; Laberty, C.; Nicole, L. *Chem. Mater.* **2008**, *20*, 682−737.
(50) Huesing, N.; Schubert, U. *Angew. Chem., Int. Ed.* **1998**, *37*, 23−45.
(51) Darhuber, A. A.; Troian, S. M.; Davis, J. M.; Miller, S. M.; Wagner, S. *J. Appl. Phys.* **2000**, *88*, 5119−5126.
(52) Landau, L.; Levich, B. *Act. Physicochim. Urss* **1942**, *17*, 42−54.
(53) Baik, D. G.; Cho, S. M. *Thin Solid Films* **1999**, *354*, 227−231.
(54) Vayssieres, L.; Keis, K.; Lindquist, S. E.; Hagfeldt, A. *J. Phys. Chem. B* **2001**, *105*, 3350−3352.
(55) Lu, X. B.; Zhang, H. J.; Ni, Y. W.; Zhang, Q.; Chen, J. P. *Biosens. Bioelectron.* **2008**, *24*, 93−98.
(56) Ruankham, P.; Macaraig, L.; Sagawa, T.; Nakazumi, H.; Yoshikawa, S. *J. Phys. Chem. C* **2011**, *115*, 23809−23816.
(57) Otsuka, A.; Funabiki, K.; Sugiyama, N.; Yoshida, T. *Chem. Lett.* **2006**, *35*, 666−667.
(58) Mor, G. K.; Kim, S.; Paulose, M.; Varghese, O. K.; Shankar, K.; Basham, J.; Grimes, C. A. *Nano Lett.* **2009**, *9*, 4250−4257.
(59) Mor, G. K.; Basham, J.; Paulose, M.; Kim, S.; Varghese, O. K.; Vaish, A.; Yoriya, S.; Grimes, C. A. *Nano Lett.* **2010**, *10*, 2387−2394.
(60) Bouclé, J.; Snaith, H. J.; Greenham, N. C. *J. Phys. Chem. C* **2010**, *114*, 3664−3674.
(61) Olson, D. C.; Shaheen, S. E.; Collins, R. T.; Ginley, D. S. *J. Phys. Chem. C* **2007**, *111*, 16670−16678.
(62) Oosterhout, S. D.; Wienk, M. M.; van Bavel, S. S.; Thiedmann, R.; Koster, L. J. A.; Gilot, J.; Loos, J.; Schmidt, V.; Janssen, R. A. J. *Nat. Mater.* **2009**, *8*, 818−824.
(63) Weickert, J.; Sun, H. Y.; Palumbiny, C.; Hesse, H. C.; Schmidt-Mende, L. *Sol. Energy Mater. Sol. Cells* **2010**, *94*, 2371−2374.